Quantum Frequency Conversion between Infrared and Ultraviolet

Helge Rütz,* Kai-Hong Luo, Hubertus Suche, and Christine Silberhorn
Integrated Quantum Optics, Applied Physics, University of Paderborn, Warburger Str. 100, 33098 Paderborn, Germany

(Received 15 July 2016; revised manuscript received 20 December 2016; published 23 February 2017)

We report on the implementation of quantum frequency conversion between infrared and ultraviolet (UV) wavelengths by using single-stage up-conversion in a periodically poled potassium-titanyl-phosphate waveguide. Because of the monolithic waveguide design, we manage to transfer a telecommunication-band input photon to the wavelength of the ionic dipole transition of Yb^+ at 369.5 nm. The external (internal) conversion efficiency is around 5% (10%). The high-energy pump used in this converter introduces a spontaneous parametric down-conversion process, which is a cause for noise in the UV mode. Using this process, we show that the converter preserves nonclassical correlations in the up-conversion process, rendering this miniaturized interface a source for quantum states of light in the UV.

DOI: 10.1103/PhysRevApplied.7.024021

I. INTRODUCTION

Quantum networks and long-distance quantum communication rely on the faithful transfer and manipulation of quantum states. Because a single quantum system does not necessarily incorporate all the benefits needed, a hybrid system [1,2] with different nodes operating at dissimilar frequencies may be used to perform each task at its optimal frequency. The process of quantum frequency conversion (QFC) [3,4] has been established as a means to bridge the gap between differing frequencies while keeping the quantum correlations intact. On the one side of that gap, telecommunication bands in the infrared spectral region have consensually been identified as the optimal wavelengths for quantum-state transfer because of low loss in optical fibers, and a multitude of experimental studies have shown QFC from [4–11] and to [12–17] the telecommunications bands, cf. Fig. 1(a). Looking at the other side of the gap, one finds that QFC experiments have, so far, mainly focused on convenient laser wavelengths or transitions in the red and near-infrared spectral region. However, high-fidelity photonic-state manipulation strongly benefits from high-energy transitions and indeed, most of the beneficial ionic transitions are situated at ultraviolet (UV) wavelengths. Most prominently, the ytterbium (Yb^+) transition at 369.5 nm constitutes an almost ideal two-level quantum system due to the Yb^+ ion's specific electronic structure [18]. It has been shown that the $S_{1/2} \rightarrow P_{1/2}$ transition can act as a photonic interface for efficient and long-lived storage of quantum bits [19], and the Yb ion proves to be useful for quantum computing [18,20] and fundamental studies of light-matter interactions [21]. While this ion is, thus, an ideal system for the manipulation of quantum states, its application for quantum networks and long-distance quantum communication in a hybrid system is conditioned on the possibility of connecting it to the optimal fiber transmission window [cf. fiber attenuation in Fig. 1(c)]. This is a challenging venture and involves significant engineering effort because of the large energy gap between input and output, as well as the properties of nonlinear materials at UV wavelengths. In contrast to a proposal to use a two-stage cavity system [22],

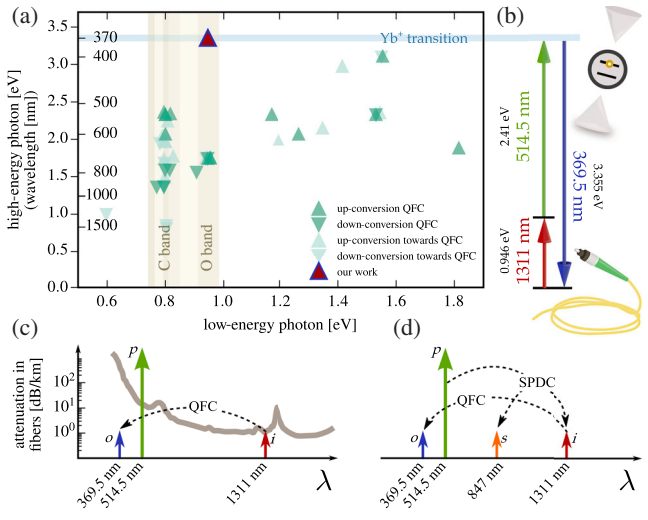

FIG. 1. Quantum frequency conversion between the telecommunication O band and the ultraviolet. The conversion to the UV wavelength of 369.5 nm (dark-edged triangle) is contrasted to state-of-the-art quantum frequency conversion (dark triangle) [3–10,12–17,24–29] as well as important work towards QFC (light triangle) [30–49] in a plot that has the input and output photon energy on its axes (a). The concept is presented on an energy (b) and wavelength (c) scale. For comparison, the attenuation in optical fibers [50], which makes direct transmission of UV light impossible, is shown (c). The concept of a cascaded SPDC/QFC process used for QFC to the UV is depicted in (d).

*helge.ruetz@uni-paderborn.de

we have recently demonstrated a classical up-conversion process in a rubidium-doped periodically poled potassium-titanyl phosphate (PPKTP) waveguide [23], which provides the basis for QFC.

In this article, we report on the QFC between infrared and UV for single-photon states. More specifically, we show QFC between the telecommunications O band (around 1310 nm) and the wavelength of the Yb^+ transition at 369.5 nm, bridging an energy gap larger than 2.4 eV (580 THz) and directly matching the $S_{1/2} \rightarrow P_{1/2}$ dipole transition in Yb^+. By converting single-photon-level light, we show an external (internal) efficiency above 5% (10%). Using an intrinsic spontaneous parametric down-conversion (SPDC) process, we verify the preservation of nonclassicality between the input and output modes. This SPDC process, on the one hand, acts as a source of noise in the conversion process, but also allows—in conjunction with the up-conversion process—the production of quantum states of light in the UV, which would otherwise require a pump at even shorter wavelengths.

II. CONCEPT

The concept of this QFC on an energy and a wavelength scale is depicted in Figs. 1(b) and 1(c), respectively. The QFC Hamiltonian is given by [51]

$$\hat{\mathcal{H}}_{\mathrm{QFC}} = i\hbar\kappa A_p \hat{a}_i \hat{a}_o^\dagger + \mathrm{H.c.}, \tag{1}$$

where $\hat{a}_{\{i,o\}}$ are annihilation operators for the input (i) and output (o) mode, A_p is the classically treated pump field, and κ is the coupling constant which incorporates the nonlinearity of the material as well as the transverse overlap of the light fields. In principle, the QFC process is noiseless and can work with unit efficiency, a fact that can be anticipated from the beam-splitter-like form of Eq. (1). In practice, however, losses and detrimental effects caused by the strong pump field limit the attainable efficiency. The noise in the converter we report on here is caused by a SPDC process as sketched in Fig. 1(d). Here, the strong pump decays into a pair of signal (s) and idler (i) photons, where the idler mode is identical to the input mode of the QFC process according to

$$\hat{\mathcal{H}}_{\mathrm{SPDC}} = i\hbar\gamma A_p \hat{a}_s^\dagger \hat{a}_i^\dagger + \mathrm{H.c.}, \tag{2}$$

where γ is the coupling constant for the SPDC process. The produced SPDC state exhibits strong nonclassical correlations [52] and these correlations are preserved in the frequency conversion process as we verify experimentally in this paper. The cascaded process of the generation and successive conversion has been studied theoretically in [53,54], and so far experimental implementations have used bright light to characterize phase matching [55] and correlations in the context of continuous variables [56,57]. The output state of such a cascaded process over time t can be calculated by the evolution $\hat{U} = \hat{U}_{\mathrm{QFC}}\hat{U}_{\mathrm{SPDC}}$ with $\hat{U}_{\mathrm{QFC}} = \exp(it\hat{\mathcal{H}}_{\mathrm{QFC}}/\hbar)$ and $\hat{U}_{\mathrm{SPDC}} = \exp(it\hat{\mathcal{H}}_{\mathrm{SPDC}}/\hbar)$,

$$\hat{U}|0_s, 0_i, 0_o\rangle \sim \gamma A_p t |1_s, 1_i, 0_o\rangle + \gamma\kappa A_p^2 t^2 |1_s, 0_i, 1_o\rangle, \tag{3}$$

showing quantum correlations between a signal and an output mode in quadratic dependence on the pump field.

III. EXPERIMENT

The implementation of QFC between the IR and the UV is based on a type-0 sum frequency generation (SFG) process with a strong pump at 514.5 nm in a PPKTP waveguide (AdvR Inc.). The waveguide has a length of $L = 9.6$ mm and the nominal poling period is $\Lambda = 2.535$ μm. The experimental setup to study this QFC is shown in Fig. 2. The waveguide chip is pumped with a continuous-wave argon ion laser in single longitudinal and spatial mode operation, while the IR input beam is produced by a tunable external cavity diode laser. Both beams are overlapped on a dichroic mirror and then launched into the waveguide, where care must be taken to excite the fundamental mode. The sample is stabilized with an accuracy of ± 4 mK around room temperature to obtain quasi-phase-matching (QPM) such that the SFG (1311 nm + 514.5 nm → 369.5 nm) takes place inside the waveguide. The exact QPM wavelength is tunable by temperature, as well as pump power, as discussed in our classical characterization [23]. Behind the waveguide, we use a dichroic mirror to separate the UV light from the pump and input light, then several successive dielectric filters (with a bandwidth of ~6 nm and a cumulative optical density above 22 at the pump wavelength) centered at 370 nm to filter out the remaining pump light.

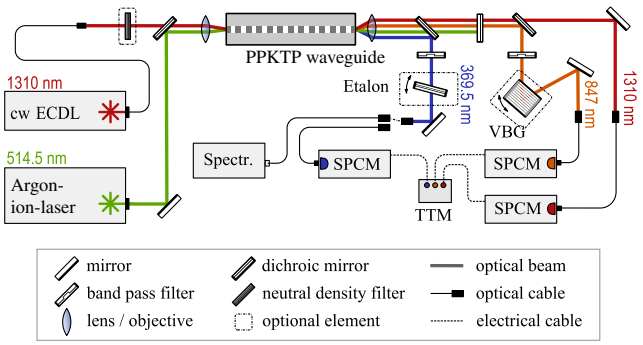

FIG. 2. Schematic of the experimental setup. Details are described in the text. The following abbreviations are used: cw ECDL, continuous-wave external-cavity diode laser; VBG, volume Bragg grating; SPCM, single-photon counting module; Spectr., sensitive spectrometer; TTM, time-tagging module. Elements surrounded by dotted lines are optionally placed into the beam path.

IV. EFFICIENCY

First, we investigate the conversion efficiency on the single-photon level and apply narrow filtering to reduce noise contributions. To this end, the generated UV light is coupled to a blue enhanced single-photon counting module (SPCM) with a dark count rate of 13 Hz. As input, we use cw light with a photon flux of $I = 6$ MHz (∼1 pW), which is compatible to state-of-the-art single-photon sources [58,59]. For evaluating the signal-to-noise ratio (SNR), $(S+N)/N$, we record the output count rate S as the number of counts within one second, averaged over ten successive measurements, as well as the noise rate N, i.e., the rate without any input. In order to increase the SNR, narrow filtering is applied, i.e., we insert a homemade etalon with a free spectral range of 340 GHz (∼150 pm at 370 nm wavelength) and a nominal bandwidth of 5.5 GHz (2.5 pm) into the beam path. In Fig. 3(a) we plot the measured SNR as a function of the pump power for the etalon filtered (nonfiltered) case as squares (diamonds) and find an SNR above 2 at pump powers up to 200 mW when using narrow filtering.

We define the external conversion efficiency η_{ext} as the number of converted photons exiting the nonlinear crystal $\langle n\rangle_{\mathrm{out}}$ divided by the number of input photons in front of it $\langle n\rangle_{\mathrm{in}}$, $\eta_{\mathrm{ext}} = \langle n\rangle_{\mathrm{out}}/\langle n\rangle_{\mathrm{in}} = (S-N)/(I\eta_{\mathrm{loss}})$, where η_{loss} accounts for optical losses outside the waveguide chip (∼22%), fiber coupling (∼69%), the detection efficiency (∼14%) and, where appropriate, the etalon transmission (∼50%). Figure 3(b) shows the pump-power-dependent conversion efficiencies at the single-photon level in the filtered (squares) and unfiltered (diamonds) case. The external conversion efficiency is $\eta_{\mathrm{ext}} = 5.5\%$ at 200 mW pump power; in this case an SNR above 2 is achieved at the detector. Considering the mode matching into the waveguide based on transmission measurements [23], we estimate an internal conversion efficiency of $\eta_{\mathrm{int}} = 10.5\%$. For both the filtered and unfiltered case, the same conversion efficiency is obtained within the range of experimental repeatability. This is in good agreement with measurements using bright input light around 20 μW [23] as an input [circles in Fig. 3(b)] showing faithful up-conversion over 7 orders of magnitude of input signal. While higher efficiencies can be observed at higher pump powers, using the converter at a pump power of 200 mW seems to be a good compromise between optimal conversion efficiency and acceptable SNR. This is especially appropriate since the conversion efficiency saturates at elevated pump powers, which we attribute to a pump-power-dependent UV absorption. Using a pulsed pump may significantly reduce this saturation effect, such that an internal efficiency up to 30% could potentially be reached for the same pump peak power levels [23]. Note that due to the symmetry of the QFC Hamiltonian, the inverse process of down-converting a UV photon to the telecommunication band in the same device can be expected to work with a similar internal efficiency—with the external efficiency solemnly limited by the technicality of diffraction-limited mode matching to the UV waveguide mode.

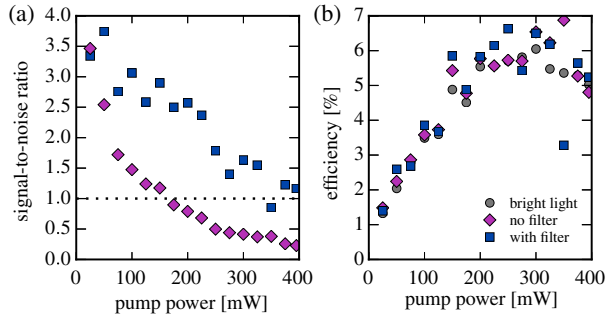

FIG. 3. Up-conversion at the single-photon level. Rates are measured as the number of counts within one second, averaged over 10 successive measurements. (a) Signal-to-noise ratio with and without etalon filtering (see text). (b) Conversion efficiency of bright (22 μW) and weak (1 pW) telecommunications band input light.

V. NOISE

We now consider the noise background stemming from SPDC in more detail. While in principle, noise in QFC can also be caused by spontaneous Raman scattering of the strong pump [60] it is not to be expected in our process as the pump is spectrally well separated from the output (> 0.9 eV). In our QFC the noise is mainly due to a cascaded SPDC/SFG process, as sketched in Fig. 1(d). In the first stage of this cascaded process, pump photons nondegenerately decay into two daughter photons, one of which, *idler* (i), is at the wavelength band of the input light around 1311 nm, the other, *signal* (s), keeps energy conservation. Subsequently, due to the QPM of the SFG process, the photon produced at the input wavelength is converted to the UV output (o) and appears as noise inside the detection band. As each of those processes is operated at low efficiency, they show a linear behavior as a function of the pump power. The cascaded process, therefore, evolves quadratically with pump power, see Eq. (3). Such a process can always happen if the pump for the QFC process is located at a wavelength shorter than the input wavelength [60,61].

The count rates without input in the filtered (unfiltered) case are shown in Fig. 4(a) as upward (downward) triangles. In the unfiltered case the count rate shows a quadratic dependence on the pump power, which is in agreement with other reported converters in the visible range [61] and can be anticipated from Eq. (3). The count rate with narrow filtering is significantly reduced and appears linear as a function of pump power. The output from the waveguide is then coupled to a spectrometer system with a resolution of about 0.15 nm. Figure 4(b) shows the spectrum when only pump light is coupled to the

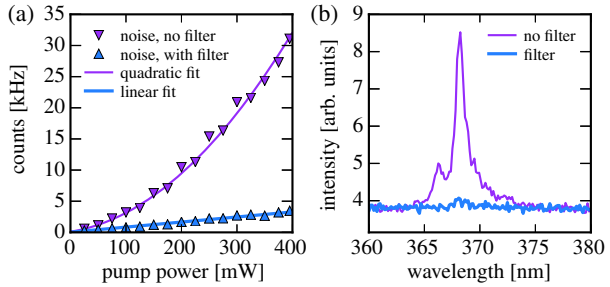

FIG. 4. Noise in single-photon level up-conversion. (a) Count rates at the wavelength of the up-converted light around 370 nm without input. (b) Spectrally resolved output noise with and without narrow etalon filtering.

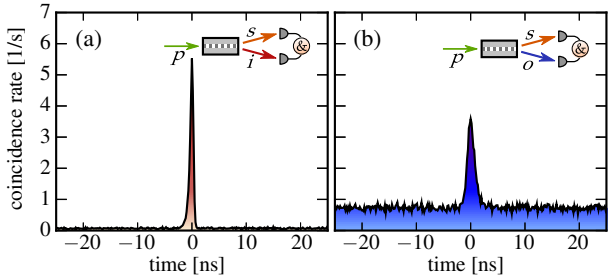

FIG. 5. Coincidence measurements. (a) Coincidence measurement between signal around 847 nm and infrared. A pump power of 400 μW, time binning of 165 ps and total measurement time of 230 s are used. (b) Coincidence measurement between signal around 847 nm and UV output. A pump power of 200 mW and total measurement time of 136 s are used.

waveguide. When no etalon is used, it shows a pronounced broadband peak and its shape resembles the phase-matching curve of the SFG process [23]. Using the etalon almost completely eliminates the peak. The remaining noise is thus very broadband and could be easily filtered out using etalon cascades. It should also be mentioned that in the envisioned usage case the atomic transition of the ion can itself act as a narrow filter to increase the SNR, i.e., within its 20-MHz bandwidth a noise count rate of only 1.3 Hz would be expected.

VI. COINCIDENCES

Finally, we measure coincidence events between the wavelengths in question, thereby showing the parametric nature of the noise and the preservation of quantum features in the frequency conversion process. By evaluating the cross-correlation between the mode at signal and idler, as well as between signal and the converted UV mode we show the nonclassicality of the state and its preservation during frequency conversion. We pump the waveguide at ~400-μW pump power and separate the near-infrared from the telecommunications O-band light. The latter is coupled to a free-running SPCM. The light around 850 nm is filtered using a bandpass filter (FWHM ~ 4 nm) and launched to another SPCM. Detector events are recorded by means of a time-tagging module. A histogram of the time difference τ between events in both channels is plotted in Fig. 5(a). A singular peak in the coincidence rate is observed, stemming from correlated SPDC photons in the two modes.

The cross-correlation function $g^{(2)}_{s,i}$ is given by $g^{(2)}_{s,i} = p_{s,i}/(p_s p_i)$, where $p_{s,i}$ is the probability for a coincidence event and p_s and p_i are the probabilities of detecting a photon in either mode [62]. In practice, this ratio is calculated by $g^{(2)}_{s,i} = r_{s,i}(\tau = 0)/r_{s,i}(\tau \neq 0)$, dividing the coincidence rate at the peak's position $r_{s,i}(\tau = 0)$ by the coincidence rate outside the coincidence window $r_{s,i}(\tau \neq 0)$. The Cauchy-Schwarz inequality $g^{(2)}_{s,i} \leq \sqrt{g^{(2)}_s(0) g^{(2)}_i(0)}$ [63], with $g^{(2)}_s(0)$ and $g^{(2)}_i(0)$ being the autocorrelation function of the two fields at zero time delay, serves as a criterion for classicality. The perfect thermal state would show an autocorrelation of 2, imperfections and noise only lowering this value towards 1, limiting $g^{(2)}_{s,i} \leq 2$ for classical states. Here, we obtain $g^{(2)}_{s,i} = 78 \pm 20$, indicating the expected nonclassicality of the SPDC state.

To measure the cross-correlation function $g^{(2)}_{s,o}$ between the signal and the output state, we increase the pump power to 200 mW, high enough for efficient conversion. In the UV beam path we use the 6-nm filters, but no etalon and couple the light to the SPCM. In the red beam path we install a volume Bragg grating (FWHM ~ 1 nm). This is necessary because the high pump power reduces the value of the cross-correlation function as more luminescence noise couples to the modes. Still, a clear peak is observed in the coincidence rates between signal and output modes, which is shown in Fig. 5(b). The cross-correlation is $g^{(2)}_{s,o} = 4.9 \pm 0.5 \not\leq 2$, violating the Cauchy-Schwarz classicality criterion by more than 5 standard deviations. Note that we would expect an even higher violation using external SPDC photons from a narrow-band source [64] due to the possibility of improved filtering of the near-infrared photons. The preservation of correlations together with the SNR above 2 make this device directly deployable for time-bin qubit conversion [4,12], while polarization qubits would require an appropriate multiplexing scheme (e.g., Sagnac loop).

VII. CONCLUSION

In conclusion, we have implemented QFC between infrared and UV wavelengths based on SFG in a PPKTP waveguide. Using a fixed single-mode pump at 514.5 nm, the device allows one to interface the telecommunication band at 1311 nm to the Yb^+ transition at 369.5 nm with an external (internal) efficiency of $\eta_{\text{ext}} = 5.5\%$ ($\eta_{\text{int}} = 10.5\%$). The device retains its conversion properties on the

single-photon level and is quantum-state preserving, which is shown by converting an intrinsic SPDC state. This intrinsic SPDC process is the main noise contribution for the conversion. However, strong filtering can notably limit its influence and an even higher noise suppression can be expected when using the ionic transition itself as a filter. The results shown in this paper pave the way towards a whole range of applications with the two most prominent ones being that our device constitutes a monolithic source for quantum states of light at UV wavelengths, which may be further improved by specifically tailoring the SPDC process, and that operating the device in the reverse direction, i.e., down-converting light from 369.5 nm to the telecommunications O band, does not pose a fundamental problem. We, therefore, expect our device to be highly useful for quantum information tasks involving direct access to trapped ion systems in the ultraviolet spectral region.

ACKNOWLEDGMENTS

We thank Stephan Krapick and Viktor Quiring for help in designing and producing the filtering etalon used in this work and Harald Herrmann for helpful discussions. We acknowledge financial support provided by the Bundesministerium für Bildung und Forschung within the *QuOReP* and *Q.com-Q* framework.

[1] H. J. Kimble, The quantum internet, Nature (London) **453**, 1023 (2008).
[2] Monika Schleier-Smith, Editorial: Hybridizing Quantum Physics and Engineering, Phys. Rev. Lett. **117**, 100001 (2016).
[3] Jianming Huang and Prem Kumar, Observation of Quantum Frequency Conversion, Phys. Rev. Lett. **68**, 2153 (1992).
[4] S. Tanzilli, W. Tittel, M. Halder, O. Alibart, P. Baldi, N. Gisin, and H. Zbinden, A photonic quantum information interface, Nature (London) **437**, 116 (2005).
[5] T. Honjo, H. Takesue, H. Kamada, Y. Nishida, O. Tadanaga, M. Asobe, and K. Inoue, Long-distance distribution of time-bin entangled photon pairs over 100 km using frequency up-conversion detectors, Opt. Express **15**, 13957 (2007).
[6] M. T. Rakher, L. Ma, O. Slattery, X. Tang, and K. Srinivasan, Quantum transduction of telecommunications-band single photons from a quantum dot by frequency upconversion, Nat. Photonics **4**, 786 (2010).
[7] Matthew T. Rakher, Lijun Ma, Marcelo Davanço, Oliver Slattery, Xiao Tang, and Kartik Srinivasan, Simultaneous Wavelength Translation and Amplitude Modulation of Single Photons from a Quantum Dot, Phys. Rev. Lett. **107**, 083602 (2011).
[8] Christina E. Vollmer, Christoph Baune, Aiko Samblowski, Tobias Eberle, Vitus Händchen, Jaromír Fiurášek, and Roman Schnabel, Quantum Up-Conversion of Squeezed Vacuum States from 1550 to 532 nm, Phys. Rev. Lett. **112**, 073602 (2014).
[9] Wenyuan Liu, Ning Wang, Zongyang Li, and Yongmin Li, Quantum frequency up-conversion of continuous variable entangled states, Appl. Phys. Lett. **107**, 231109 (2015).
[10] Zhi-Yuan Zhou, Yan Li, Dong-Sheng Ding, Wei Zhang, Shuai Shi, Bao-Sen Shi, and Guang-Can Guo, Orbital angular momentum photonic quantum interface, Light Sci. Appl. **5**, e16019 (2016).
[11] Christoph Baune, Jan Gniesmer, Sacha Kocsis, Christina E. Vollmer, Petrissa Zell, Jaromír Fiurášek, and Roman Schnabel, Unconditional entanglement interface for quantum networks, Phys. Rev. A **93**, 010302 (2016).
[12] Rikizo Ikuta, Yoshiaki Kusaka, Tsuyoshi Kitano, Hiroshi Kato, Takashi Yamamoto, Masato Koashi, and Nobuyuki Imoto, Wide-band quantum interface for visible-to-telecommunication wavelength conversion, Nat. Commun. **2**, 1544 (2011).
[13] Sebastian Zaske, Andreas Lenhard, Christian A. Keßler, Jan Kettler, Christian Hepp, Carsten Arend, Roland Albrecht, Wolfgang-Michael Schulz, Michael Jetter, Peter Michler, and Christoph Becher, Visible-to-Telecom Quantum Frequency Conversion of Light from a Single Quantum Emitter, Phys. Rev. Lett. **109**, 147404 (2012).
[14] Kristiaan De Greve, Leo Yu, Peter L. McMahon, Jason S. Pelc, Chandra M. Natarajan, Na Young Kim, Eisuke Abe, Sebastian Maier, Christian Schneider, Martin Kamp, Sven Höfling, Robert H. Hadfield, Alfred Forchel, M. M. Fejer, and Yoshihisa Yamamoto, Quantum-dot spin-photon entanglement via frequency downconversion to telecom wavelength, Nature (London) **491**, 421 (2012).
[15] Jason S. Pelc, Leo Yu, Kristiaan De Greve, Peter L. McMahon, Chandra M. Natarajan, Vahid Esfandyarpour, Sebastian Maier, Christian Schneider, Martin Kamp, Sven Höfling, Robert H. Hadfield, Alfred Forchel, Yoshihisa Yamamoto, and M. M. Fejer, Downconversion quantum interface for a single quantum dot spin and 1550-nm single-photon channel, Opt. Express **20**, 27510 (2012).
[16] Boris Albrecht, Pau Farrera, Xavier Fernandez-Gonzalvo, Matteo Cristiani, and Hugues de Riedmatten, A waveguide frequency converter connecting rubidium-based quantum memories to the telecom C-band, Nat. Commun. **5**, 3376 (2014).
[17] Leo Yu, Chandra M. Natarajan, Tomoyuki Horikiri, Carsten Langrock, Jason S. Pelc, Michael G. Tanner, Eisuke Abe, Sebastian Maier, Christian Schneider, Sven Hfling, Martin Kamp, Robert H. Hadfield, Martin M. Fejer, and Yoshihisa Yamamoto, Two-photon interference at telecom wavelengths for time-bin-encoded single photons from quantum-dot spin qubits, Nat. Commun. **6**, 8955 (2015).
[18] S. Olmschenk, D. Hayes, D. N. Matsukevich, P. Maunz, D. L. Moehring, and C. Monroe, Quantum logic between distant trapped ions, Int. J. Quantum. Inform. **08**, 337 (2010).
[19] S. Olmschenk, K. C. Younge, D. L. Moehring, D. N. Matsukevich, P. Maunz, and C. Monroe, Manipulation and detection of a trapped Yb^+ hyperfine qubit, Phys. Rev. A **76**, 052314 (2007).
[20] Th. Hannemann, D. Reiss, Ch. Balzer, W. Neuhauser, P. E. Toschek, and Ch. Wunderlich, Self-learning estimation of quantum states, Phys. Rev. A **65**, 050303 (2002).
[21] Robert Maiwald, Andrea Golla, Martin Fischer, Marianne Bader, Simon Heugel, Benoît Chalopin, Markus Sondermann, and Gerd Leuchs, Collecting more than half

the fluorescence photons from a single ion, Phys. Rev. A **86**, 043431 (2012).

[22] Ryan Clark, Taehyun Kim, and Jungsang Kim, Double-stage frequency down-conversion system for distribution of ion-photon entanglement over long distances, in *Proceedings of the 2011 IEEE Photonics Society Summer Topical Meeting Series* (IEEE, New York, 2011).

[23] Helge Rütz, Kai-Hong Luo, Hubertus Suche, and Christine Silberhorn, Towards a quantum interface between telecommunication and UV wavelengths: Design and classical performance, Appl. Phys. B **122**, 13 (2016).

[24] Serkan Ates, Imad Agha, Angelo Gulinatti, Ivan Rech, Matthew T. Rakher, Antonio Badolato, and Kartik Srinivasan, Two-Photon Interference Using Background-Free Quantum Frequency Conversion of Single Photons Emitted by an InAs Quantum Dot, Phys. Rev. Lett. **109**, 147405 (2012).

[25] Dehuan Kong, Zongyang Li, Shaofeng Wang, Xuyang Wang, and Yongmin Li, Quantum frequency down-conversion of bright amplitude-squeezed states, Opt. Express **22**, 24192 (2014).

[26] S. Ramelow, A. Fedrizzi, A. Poppe, N. K. Langford, and A. Zeilinger, Polarization-entanglement-conserving frequency conversion of photons, Phys. Rev. A **85**, 013845 (2012).

[27] H. J. McGuinness, M. G. Raymer, C. J. McKinstrie, and S. Radic, Quantum Frequency Translation of Single-Photon States in a Photonic Crystal Fiber, Phys. Rev. Lett. **105**, 093604 (2010).

[28] John M. Donohue, Jonathan Lavoie, and Kevin J. Resch, Ultrafast Time-Division Demultiplexing of Polarization-Entangled Photons, Phys. Rev. Lett. **113**, 163602 (2014).

[29] A. G. Radnaev, Y. O. Dudin, R. Zhao, H. H. Jen, S. D. Jenkins, A. Kuzmich, and T. A. B. Kennedy, A quantum memory with telecom-wavelength conversion, Nat. Phys. **6**, 894 (2010).

[30] Aaron P. Vandevender and Paul G. Kwiat, High efficiency single photon detection via frequency up-conversion, J. Mod. Opt. **51**, 1433 (2004).

[31] Marius A. Albota and Franco N. C. Wong, Efficient single-photon counting at 1.55 μm by means of frequency upconversion, Opt. Lett. **29**, 1449 (2004).

[32] R. T. Thew, S. Tanzilli, L. Krainer, S. C. Zeller, A. Rochas, I. Rech, S. Cova, H. Zbinden, and N. Gisin, Low jitter up-conversion detectors for telecom wavelength GHz QKD, New J. Phys. **8**, 32 (2006).

[33] Carsten Langrock, Eleni Diamanti, Rostislav V. Roussev, Yoshihisa Yamamoto, M. M. Fejer, and Hiroki Takesue, Highly efficient single-photon detection at communication wavelengths by use of upconversion in reverse-proton-exchanged periodically poled $LiNbO_3$ waveguides, Opt. Lett. **30**, 1725 (2005).

[34] Paulina S. Kuo, Jason S. Pelc, Oliver Slattery, Yong-Su Kim, M. M. Fejer, and Xiao Tang, Reducing noise in single-photon-level frequency conversion, Opt. Lett. **38**, 1310 (2013).

[35] Jeff T. Hill, Amir H. Safavi-Naeini, Jasper Chan, and Oskar Painter, Coherent optical wavelength conversion via cavity optomechanics, Nat. Commun. **3**, 1196 (2012).

[36] Amy C. Turner-Foster, Mark A. Foster, Reza Salem, Alexander L. Gaeta, and Michal Lipson, Frequency conversion over two-thirds of an octave in silicon nanowaveguides, Opt. Express **18**, 1904 (2010).

[37] Rostislav V. Roussev, Carsten Langrock, Jonathan R. Kurz, and M. M. Fejer, Periodically poled lithium niobate waveguide sum-frequency generator for efficient single-photon detection at communication wavelengths, Opt. Lett. **29**, 1518 (2004).

[38] Alex S. Clark, Shayan Shahnia, Matthew J. Collins, Chunle Xiong, and Benjamin J. Eggleton, High-efficiency frequency conversion in the single-photon regime, Opt. Lett. **38**, 947 (2013).

[39] Hiroki Takesue, Single-photon frequency down-conversion experiment, Phys. Rev. A **82**, 013833 (2010).

[40] J. S. Pelc, L. Ma, C. R. Phillips, Q. Zhang, C. Langrock, O. Slattery, X. Tang, and M. M. Fejer, Long-wavelength-pumped upconversion single-photon detector at 1550 nm: Performance and noise analysis, Opt. Express **19**, 21445 (2011).

[41] Noé Curtz, Rob Thew, Christoph Simon, Nicolas Gisin, and Hugo Zbinden, Coherent frequency-down-conversion interface for quantum repeaters, Opt. Express **18**, 22099 (2010).

[42] Benjamin Brecht, Andreas Eckstein, Raimund Ricken, Viktor Quiring, Hubertus Suche, Linda Sansoni, and Christine Silberhorn, Demonstration of coherent time-frequency Schmidt mode selection using dispersion-engineered frequency conversion, Phys. Rev. A **90**, 030302 (2014).

[43] Fabian Steinlechner, Nathaniel Hermosa, Valerio Pruneri, and Juan P. Torres, Frequency conversion of structured light, Sci. Rep. **6**, 21390 (2016).

[44] Xiaorong Gu, Kun Huang, Haifeng Pan, E Wu, and Heping Zeng, Photon correlation in single-photon frequency up-conversion, Opt. Express **20**, 2399 (2012).

[45] G. Giorgi, P. Mataloni, and F. De Martini, Frequency Hopping in Quantum Interferometry: Efficient Up-Down Conversion for Qubits and Ebits, Phys. Rev. Lett. **90**, 027902 (2003).

[46] Yu Ding and Z. Y. Ou, Frequency downconversion for a quantum network, Opt. Lett. **35**, 2591 (2010).

[47] Sebastian Zaske, Andreas Lenhard, and Christoph Becher, Efficient frequency downconversion at the single photon level from the red spectral range to the telecommunications C-band, Opt. Express **19**, 12825 (2011).

[48] Rikizo Ikuta, Toshiki Kobayashi, Shuto Yasui, Shigehito Miki, Taro Yamashita, Hirotaka Terai, Mikio Fujiwara, Takashi Yamamoto, Masato Koashi, Masahide Sasaki, Zhen Wang, and Nobuyuki Imoto, Frequency down-conversion of 637 nm light to the telecommunication band for non-classical light emitted from NV centers in diamond, Opt. Express **22**, 11205 (2014).

[49] Y.-H. Cheng, Tim Thomay, Glenn S. Solomon, Alan L. Migdall, and Sergey V. Polyakov, Statistically background-free, phase-preserving parametric up-conversion with faint light, Opt. Express **23**, 18671 (2015).

[50] Andreas Langner, Gerhard Schötz, and Jan Vydra, Speciality fibers for light transmission from UV to IR, Photonik International **1**, 10 (2007).

[51] Prem Kumar, Quantum frequency conversion, Opt. Lett. **15**, 1476 (1990).

[52] Christopher Gerry and Peter Knight, *Introductory Quantum Optics* (Cambridge University Press, Cambridge, 2004).

[53] E. A. Mishkin and D. F. Walls, Quantum statistics of three interacting boson field modes, Phys. Rev. **185**, 1618 (1969).
[54] Martin E. Smithers and Eugene Y. C. Lu, Quantum theory of coupled parametric down-conversion and up-conversion with simultaneous phase matching, Phys. Rev. A **10**, 1874 (1974).
[55] R. A. Andrews, Herbert Rabin, and C. L. Tang, Coupled Parametric Downconversion and Upconversion with Simultaneous Phase Matching, Phys. Rev. Lett. **25**, 605 (1970).
[56] Alessandro Ferraro, Matteo G. A. Paris, Maria Bondani, Alessia Allevi, Emiliano Puddu, and Alessandra Andreoni, Three-mode entanglement by interlinked nonlinear interactions in optical $\chi(2)$ media, J. Opt. Soc. Am. B **21**, 1241 (2004).
[57] Alessia Allevi, Maria Bondani, Matteo G. A. Paris, and Alessandra Andreoni, Demonstration of a bright and compact source of tripartite nonclassical light, Phys. Rev. A **78**, 063801 (2008).
[58] Stefan Strauf, Nick G. Stoltz, Matthew T. Rakher, Larry A. Coldren, Pierre M. Petroff, and Dirk Bouwmeester, High-frequency single-photon source with polarization control, Nat. Photonics **1**, 704 (2007).
[59] Enrico Pomarico, Bruno Sanguinetti, Thiago Guerreiro, Rob Thew, and Hugo Zbinden, MHz rate and efficient synchronous heralding of single photons at telecom wavelengths, Opt. Express **20**, 23846 (2012).
[60] J. S. Pelc, C. Langrock, Q. Zhang, and M. M. Fejer, Influence of domain disorder on parametric noise in quasi-phase-matched quantum frequency converters, Opt. Lett. **35**, 2804 (2010).
[61] Nicolas Maring, Kutlu Kutluer, Joachim Cohen, Matteo Cristiani, Margherita Mazzera, Patrick M. Ledingham, and Hugues de Riedmatten, Storage of up-converted telecom photons in a doped crystal, New J. Phys. **16**, 113021 (2014).
[62] John F. Clauser, Experimental distinction between the quantum and classical field-theoretic predictions for the photoelectric effect, Phys. Rev. D **9**, 853 (1974).
[63] M. D. Reid and D. F. Walls, Violations of classical inequalities in quantum optics, Phys. Rev. A **34**, 1260 (1986).
[64] Kai-Hong Luo, Harald Herrmann, Stephan Krapick, Benjamin Brecht, Raimund Ricken, Viktor Quiring, Hubertus Suche, Wolfgang Sohler, and Christine Silberhorn, Direct generation of genuine single-longitudinal-mode narrowband photon pairs, New J. Phys. **17**, 073039 (2015).